Nonlocal elasticity near jamming in frictionless soft spheres

Baumgarten, Karsten; Vagberg, D.L.S.; Tighe, Brian P.

DOI
10.1103/PhysRevLett.118.098001

Publication date
2017

Document Version
Final published version

Published in
Physical Review Letters

Nonlocal Elasticity near Jamming in Frictionless Soft Spheres

Karsten Baumgarten,* Daniel Vågberg, and Brian P. Tighe
Delft University of Technology, Process & Energy Laboratory, Leeghwaterstraat 39, 2628 CB Delft, The Netherlands
(Received 25 August 2016; revised manuscript received 3 November 2016; published 27 February 2017)

We use simulations of frictionless soft sphere packings to identify novel constitutive relations for linear elasticity near the jamming transition. By forcing packings at varying wavelengths, we directly access their transverse and longitudinal compliances. These are found to be wavelength dependent, in violation of conventional (local) linear elasticity. Crossovers in the compliances select characteristic length scales, which signify the appearance of nonlocal effects. Two of these length scales diverge as the pressure vanishes, indicating that critical effects near jamming control the breakdown of local elasticity. We expect these nonlocal constitutive relations to be applicable to a wide range of weakly jammed solids, including emulsions, foams, and granulates.

DOI: 10.1103/PhysRevLett.118.098001

Classical linear elastic continuum theory is blind to structure: it contains no length scale(s) characteristic of, e.g., interparticle interactions or structural correlations [1]. As a result, the theory is only valid at asymptotically long wavelengths. While predicted displacement fields can be accurate down to a few lattice constants in ordered solids, deviations in amorphous materials are apparent over much longer distances [2,3]. Soft sphere packings, a standard model for emulsions, foams, and granular materials, provide an important example of this effect. Response functions in simulated packings depart significantly from elasticity [4–6] when the packings are close to the (un) jamming transition at zero confining pressure p [7,8].

Jammed solids are anomalously soft: while their shear modulus $G_0 \sim p^{1/2}$ vanishes continuously, the bulk modulus K_0 jumps discontinuously to zero at the jamming point. The vibrational density of states also displays excess low frequency modes with a characteristic scale $\omega^* \sim p^{1/2}$. Together with a linear dispersion relation, these features imply that longitudinal and transverse sound are characterized by diverging length scales $l^* \sim K_0^{1/2}/\omega^* \sim 1/p^{1/2}$ and $l_c \sim G_0^{1/2}/\omega^* \sim 1/p^{1/4}$, respectively [9,10]. Details remain controversial, but there is consensus that the breakdown of classical elasticity near jamming is governed by l^* [4], l_c [5], or both [6].

In order to determine the response of jammed solids at short wavelengths, one typically gives up on continuum descriptions and turns to computationally expensive methods that resolve discrete particles, such as molecular dynamics, with resulting restrictions on accessible system sizes. Here, we show that, close to jamming, continuum elasticity can be extended to short wavelengths and the considerable computational advantages of continuum methods can be retained by using nonlocal constitutive relations, which "know about" microstructure by incorporating at least one length scale ℓ [11–14]. Our work is inspired by recent demonstrations that nonlocal effects play a central role in *rheology* near jamming [15–27], and in particular by the successful application of nonlocal models to predict unusual phenomena such as flow below the nominal yield stress [19,28] and wide shear bands in split-bottomed Couette cells [29,30].

Nonlocal linear elastic constitutive relations replace the usual moduli with kernels in an integral relation [12]. This can be illustrated with a classical scalar constitutive relation $\sigma = C_0\epsilon$ in one dimension, which relates the stress σ to the strain ϵ via a modulus C_0 and holds at each position x in a volume Ω. Its nonlocal counterpart $\sigma(x) = \int_\Omega C(x-x')\epsilon(x')\mathrm{d}x'$ introduces a kernel $C(x)$. The kernel is *a priori* unknown, though it must vanish as $x \to \infty$ and must be an even-valued function in isotropic systems. The integral constitutive relation can be approximated with a weakly nonlocal or stress gradient form $(1-\ell^2\partial^2)\sigma = C_0\epsilon$. (Strain gradient variations are also possible.) In this simpler form, all nonlocal effects are quantified by the coefficient ℓ, which has units of length. To characterize and quantify nonlocal effects in a material, one must determine ℓ, or more generally its full kernel. We do so by measuring the wave-number-dependent compliance $\hat{S}(q) = 1/\hat{C}(q)$, where $\hat{C}(q)$ is the Fourier

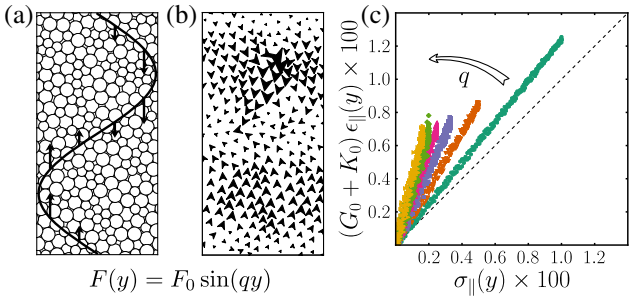

FIG. 1. (a) Sinusoidal forcing applied to a soft sphere packing, and (b) the resulting displacements. (c) A parametric plot of the constitutive relation is linear with a slope that increases with wave number q, violating classical elasticity (dashed line).

transform of $C(x)$. In a tensorial theory for isotropic materials, the kernel is not a scalar but a rank 4 tensor with two independent elements, which can be determined by measuring two separate compliances.

In the typical approach to nonlocal modeling, one uses data fitting to determine free parameters in a particular model. This can make it difficult to discriminate between the many available models [11–16,18–20,23,25–30]. Our method more closely resembles oscillatory rheology, which gives direct access to frequency-dependent viscoelastic moduli without fitting to a model. Here, we apply forcing that is periodic in space, rather than time, thereby measuring wavelength-dependent compliances [31,32] without invoking the fluctuation-dissipation relation [33]. On the basis of our measurements, we identify two diverging length scales, growing fluctuations, and new nonlocal constitutive relations.

Model system.— We study mixtures of N soft disks in $D = 2$ dimensions with equal numbers of large and small disks having a 1.4:1 ratio of their radii, a commonly studied model system [7,34]. Unless noted otherwise, $N = 65\,536$ prior to removing nonload bearing "rattlers". Contacting disks labeled i and j interact via a pair potential $V_{ij} = (1/2)k\delta_{ij}^2$, where δ_{ij} is the difference between the sum of the disks' radii and their center-to-center distance. Noncontacting disks do not interact. All results are reported in units where the spring constant k and the small particle diameter d are equal to 1. Packings are prepared in a biperiodic $L \times L$ cell via instantaneous quench from infinite to zero temperature using a nonlinear conjugate gradient method [35], followed by a series of small volume changes to reach a target pressure. Particle displacements are determined by inverting DN coupled linear equations involving the Hessian, the matrix of second derivatives of the potential energy with respect to the particle positions [36,37]. The response is calculated for vanishing perturbation amplitude, so contact changes and other nonlinear effects are absent. However, recent work has shown that the Hessian accurately predicts average stress-strain curves over finite strain intervals with an extensive number of contact changes [38–42]. We employ the standard technique of "removing the prestress", which is equivalent to replacing each contact with a spring at its rest length [43,44]. Data with the prestress are qualitatively similar but noisier. While all our simulations are in D = 2 dimensions, we expect no qualitative differences for D $\geq$ 3, because the upper critical dimension for jamming is 2 [39].

Measuring nonlocal constitutive relations.— We adapt a method developed independently by several authors—see Refs. [6,45] and especially [31,32], which explicitly make the connection to nonlocality. Packings are subjected to longitudinal and transverse force densities

$$\mathbf{f}_{\parallel}(y) = (0, f_{\parallel})^T \sin qy \tag{1}$$

$$\mathbf{f}_{\perp}(y) = (f_{\perp}, 0)^T \sin qy \tag{2}$$

with wave number q. These establish changes in the stress tensor with Fourier amplitudes $\delta\hat{\sigma}_{yy}(q) \equiv \hat{\sigma}_{\parallel}(q) = f_{\parallel}/q$ and $\delta\hat{\sigma}_{xy}(q) \equiv \hat{\sigma}_{\perp}(q) = f_{\perp}/q$, respectively. We then measure the average displacement fields $\mathbf{u}_{\parallel} = (0, u_{\parallel})^T$ and $\mathbf{u}_{\perp} = (u_{\perp}, 0)^T$. Longitudinal forcing and response are illustrated in Figs. 1(a) and 1(b). We restrict ourselves to linear response [40,42], though application to nonlinear response and flow is possible.

In a classical and isotropic elastic continuum, a sinusoidal force density establishes a sinusoidal displacement field in phase with the forcing. Hence, we can reproduce the constitutive relation by noting that a parametric plot of, e.g., the y components of $q\mathbf{u}_{\parallel}(y)$ and $q^{-1}\mathbf{f}_{\parallel}(y)$ sweeps out the same curve as a conventional plot of strain $\epsilon_{\parallel}$ vs stress $\sigma_{\parallel}$. (This is simplest to see in a scalar 1D model, where the force density $f = -\partial\sigma$ and the strain $\epsilon = \partial u$.) Classical elasticity predicts the curve will be linear with a constant slope $K_0 + G_0$ in two dimensions. The slope is independent of q because the theory is insensitive to gradients. In Fig. 1(c), we demonstrate that the second prediction fails near jamming: the slope varies with q and approaches the classical prediction (dashed line) only as $q \to 0$, when spatial gradients are weakest. This is our first main result: the elasticity of jammed packings is indeed nonlocal.

To quantify nonlocality, we measure the longitudinal compliance $\hat{S}_{\parallel}(q) = q^2\hat{u}_{\parallel}(q)/f_{\parallel}$ and transverse compliance $\hat{S}_{\perp}(q) = q^2\hat{u}_{\perp}(q)/f_{\perp}$ for each packing via direct Fourier transform of the displacement field. These two compliances fully determine the linear nonlocal constitutive relation [12], which in Fourier space reads $\hat{\sigma}_{\alpha\beta}(\mathbf{q}) = \hat{C}_{\alpha\beta\gamma\delta}(\mathbf{q})\hat{\epsilon}_{\gamma\delta}(\mathbf{q})$ (summation implied). Because of several symmetries, in isotropic materials, the tensor $\hat{C}$ has just two independent elements [1]; these are fixed by $\hat{S}_{\parallel}$ and $\hat{S}_{\perp}$. Full expressions are given in the Supplemental Material [46]. Because local elasticity must be recovered for spatially uniform strains, the compliances at $q = 0$ encode the bulk and shear modulus, $\hat{S}_{\parallel}(0) = 1/[K_0 + G_0]$ and $\hat{S}_{\perp}(0) = 1/G_0$. Continuity of the $q = 0$ limit is not required, but will be verified numerically.

Mean response.— We first consider the response to longitudinal forcing. Figure 2 depicts $S_{\parallel}(q)$ for a range of pressures close to jamming and wave numbers $2\pi/L \leq q \leq \pi/d$. Data are averaged over approximately 1000 configurations per condition.

Each curve approaches a pressure-dependent plateau $\hat{S}_{\parallel}(0^+)$ as q tends to zero. To determine whether the limit is continuous, we measure the local compliance $\hat{S}_{\parallel}(0)$ by subjecting each packing to a uniform stress in an independent test [37]. As shown in Fig. 2(b), the excess compliance $\Delta\hat{s}_{\parallel}(q) \equiv \langle\hat{S}_{\parallel}(q)/\hat{S}_{\parallel}(0)\rangle - 1$ vanishes continuously with q, indicating a continuous limit.

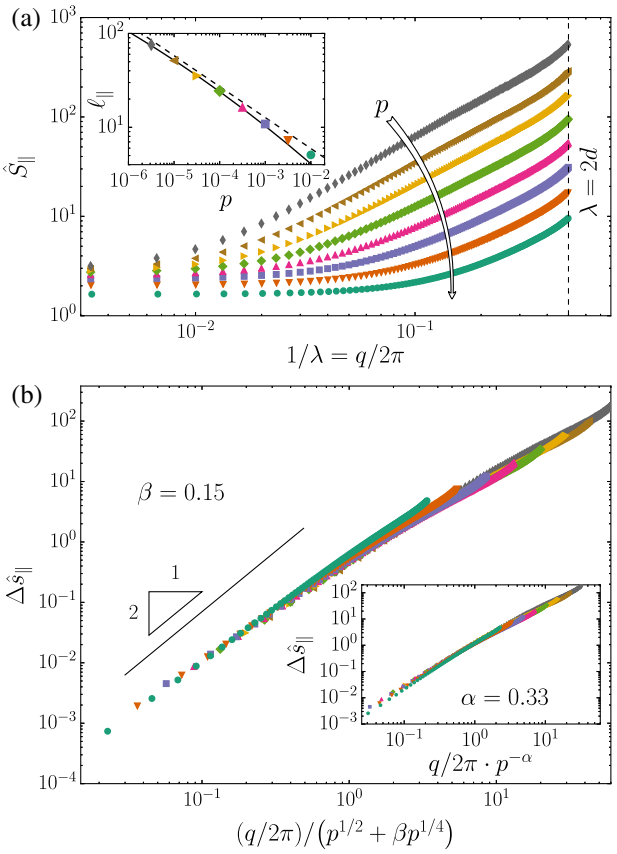

FIG. 2. (a) Longitudinal compliance $\hat{S}_\parallel(q)$ vs inverse wavelength λ for pressures $10^{-5.5} \le p \le 10^{-2}$ in half decade steps. (inset) Nonlocal length scale determined from $\hat{S}_\parallel(2\pi/\ell_\parallel)/\hat{S}_\parallel(0) = 2$. (b) Data collapse of the excess compliance $\Delta\hat{s}_\parallel(q)$ for mixed (main panel) and pure power law rescaling (inset).

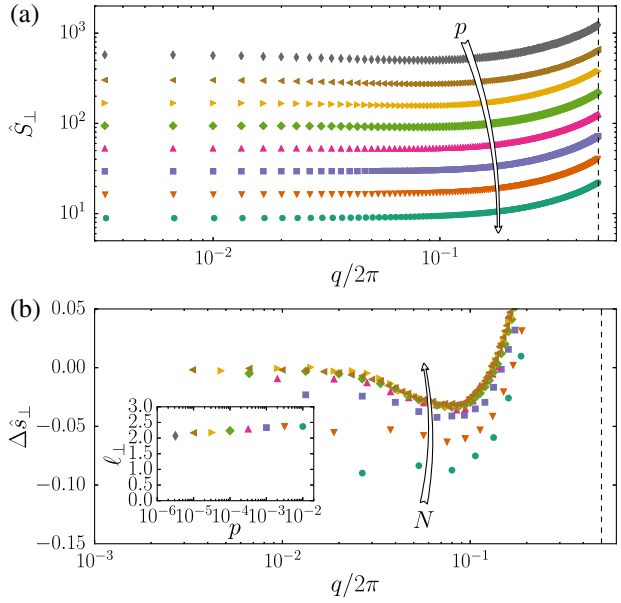

FIG. 3. (a) The transverse compliance shows no pressure-dependent crossover for $10^{-5.5} \le p \le 10^{-2}$. (b) The excess compliance at low p is nonmonotonic, even at large system size N. Here: $p = 10^{-4}$ and $2^{10} \le N \le 2^{16}$. (inset) Nonlocal length scale determined from $\hat{S}_\perp(2\pi/\ell_\perp)/\hat{S}_\perp(0) = 2$.

As q increases the compliance shows a clear pressure-dependent crossover, which selects a nonlocal length scale $\ell_\parallel$. We now show that this length diverges with pressure. To do so, we demonstrate that the excess compliance $\Delta\hat{s}_\parallel$ collapses to a master curve when plotted vs the rescaled coordinate $q\ell_\parallel$. We first consider a simple power law ansatz $\ell_\parallel \sim 1/p^\alpha$, which gives excellent data collapse for $\alpha = 0.33$ and pressures $10^{-5.5} \le p \le 10^{-3}$ [Fig. 2(b), inset]. The value of α is surprising insofar as it differs from the exponents $1/2$ and $1/4$ of the previously identified length scales l^* and l_c, respectively. Indeed, we show below that l^* and l_c can be identified in the fluctuations about the mean response. If one insists that $\ell_\parallel$ should approach l^* or l_c near jamming, it is also possible to obtain good data collapse of $\Delta\hat{s}_\parallel$ by making the alternative ansatz $1/\ell_\parallel \sim 1/l^* + \beta/l_c \sim p^{1/2} + \beta p^{1/4}$—see Fig. 2(b) (main panel). For $\beta = 0.15$ and $10^{-5.5} \le p \le 10^{-2}$, the ansatz is nearly indistinguishable from pure power law scaling [dashed and solid lines in Fig. 2(a), inset]. Hence, it is plausible $\ell_\parallel \to l_c$ (α approaches $1/4$) as $p \to 0$. We stress that a diverging nonlocal length implies significant nonlocal corrections to classical elasticity, regardless of the value of its exponent.

We now consider transverse forcing. Figure 3 plots the transverse compliance $\hat{S}_\perp(q)$ for a range of pressures. While the general shape of the compliance curves echoes the longitudinal case, there are several differences. First, the crossover scale $1/\ell_\perp$ is a constant on the order of the inverse particle size, independent of pressure. Hence, the transverse length $\ell_\perp$ does not diverge near jamming, unlike $\ell_\parallel$. A similar p-independent crossover was noted in Ref. [6] without making the connection to nonlocality. The transverse compliance is nonmonotonic, with an initial dip that appears to survive in the infinite system size limit [Fig. 3(b)]. Despite the dip, the $q \to 0$ limit is again continuous, $\hat{S}_\perp(0^+) = \hat{S}_\perp(0)$. Finite size effects are stronger than in the longitudinal forcing case (not shown); they are also more dramatic than finite size effects under uniform strain [47], which can be neglected when $p \gg 1/N^2$—which holds for all data in Fig. 3.

Constitutive relations.— For analytical modeling, it is often desirable to assign a functional form to the compliances. While one would like to have an accurate description of the nonlocal compliances over the whole range of q, no currently available nonlocal model correctly predicts the data of Figs. 2 and 3. Fitting functions are an option, though they lack physical insight. Micromechanical models such as effective medium theory (EMT) would be preferable [48]. While we expect that EMT can predict the nonlocal transverse compliance, it fails to capture the longitudinal compliance even for spatially uniform forcing [49].

Approaches based on spatially fluctuating moduli may provide an alternative [33,50–52].

Even in the absence of a more detailed model, it is possible to write down constitutive relations that capture essential nonlocal features of the mean response. As isotropy of the material requires $\hat{S}_\parallel$ and $\hat{S}_\perp$ to be even in q, the leading term in an expansion of the excess compliance is quadratic, as verified in Fig. 2(b). Truncating the expansion leads to weakly nonlocal, or stress gradient, constitutive relations, with a particularly simple form when the wave vector has fixed orientation,

$$(1 - \ell_\perp^2 \partial^2)\sigma_\perp = 2G_0 \epsilon_\perp \tag{3}$$

$$(1 - \ell_\parallel^2 \partial^2)\sigma_\parallel = (K_0 + G_0)\epsilon_\parallel. \tag{4}$$

Full expressions are available in the Supplemental Material [46]. These relations represent a qualitative improvement over classical elasticity near jamming. Equation (3) provides a good description of the transverse response over a wide range of q; note the minus sign neglects the dip in $\hat{S}_\perp$. Equation (4) introduces the diverging length scale $\ell_\parallel$, though it misses the slow bending over of $\Delta\hat{s}_\parallel$ apparent in Fig. 2(b).

Fluctuations.— It is apparent from Fig. 1(b) that individual particle displacements deviate from perfect sinusoidal response. These nonaffine fluctuations can be quantified by the ensemble average of the ratio

$$\mathcal{F}_\circ(q';q) = \left| \frac{\langle u_\circ(q)|q'_\circ\rangle}{\langle u_\circ(q)|q_\circ\rangle} \right|, \tag{5}$$

where $\circ$ refers to $\parallel$ or $\perp$. $\mathcal{F}_\circ$ compares the projections of the DN-component displacement vector $|u_\circ(q)\rangle = \{(\mathbf{u}_\circ)_i\}_{i=1\ldots N}$ on sinusoids with wave numbers $q' \neq q$ and q. The sinusoids' polarization matches the forcing. We first consider transverse forcing. We restrict our focus to long wavelengths $q \leq 30(2\pi/L)$, where $S_\perp$ is approximately flat, and consider only $q' < q$, where fluctuation amplitudes are largest. Figure 4(a) (inset) shows that for a given pressure, $\mathcal{F}_\perp$ collapses when plotted vs q'/q. The curves present a pressure-dependent crossover from steep to shallow decay. The data can be collapsed further still by plotting $p^{a_\perp}\mathcal{F}_\perp$ vs $(q'/q)/p^{1/4}$, with $a_\perp \approx 0.52$ [Fig. 4(a), main panel]. We conclude that transverse fluctuations are governed by the length scale l_c.

Analyzing low-q fluctuations under longitudinal forcing is more difficult due to the vanishing crossover near jamming. As a compromise, we vary q' and q for $q' < q \leq 10(2\pi/L)$, where the excess compliance $\Delta\hat{s}_\parallel$ is approximately quadratic for all accessed pressures. These fluctuations have a more complex dependence on q, as evidenced by slight but systematic spread in the data when plotted vs q'/q—see Fig. 4(b) (inset). Nevertheless, there is again a clear p-dependent crossover, which can be collapsed by plotting $p^{a_\parallel}\mathcal{F}_\parallel$ vs $(q'/q)/p^{1/2}$, with $a_\parallel \approx 0.57$ (main panel). While the collapse is less convincing than $\mathcal{F}_\perp$, it suggests that longitudinal fluctuations are governed by the length scale l^*.

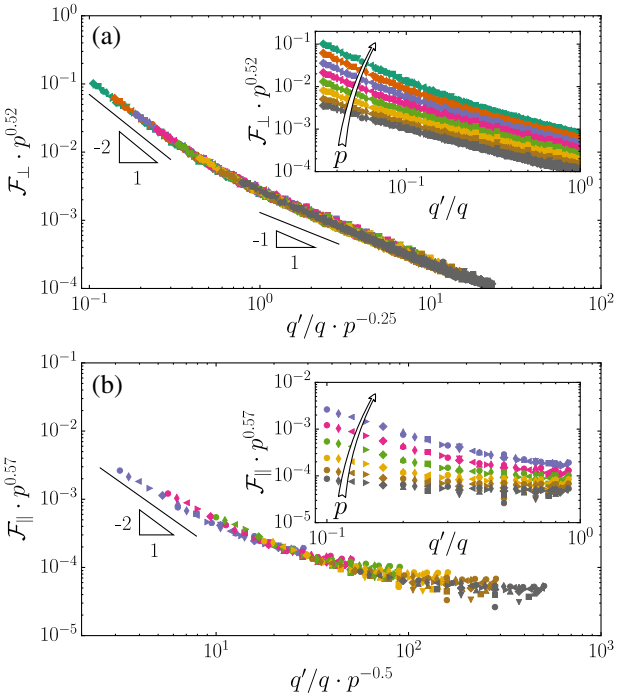

FIG. 4. (a) Data collapse of the transverse Fourier spectrum before (inset) and after (main panel) rescaling q' with $p^{-0.25}$. (b) The longitudinal Fourier spectrum shows similar collapse before (inset) and after (main panel) rescaling q' with $p^{-0.5}$.

For both types of forcing, we observe data collapse only for sufficiently low q'. The restriction to $q' < q$ is strictly necessary in the longitudinal case; data fall off the master curve rapidly for larger q'. In the transverse case the fall off comes later and more gradually. We note that prior work has related l^* [4], l_c [5], or both [6] to (deviations from) classical elastic Green's functions [4–6].

Discussion.— We have demonstrated novel constitutive relations that improve on classical elasticity near jamming by capturing the appearance of a diverging length scale within a continuum description. The divergence scales with the distance to jamming, indicating that critical effects enhance deviations from local elasticity. Nonlocal effects are stronger in deformations involving compression, as reflected in the distinct length scales $\ell_\perp$ and $\ell_\parallel$; the former remains finite, while the latter diverges. Fluctuations about the mean nonlocal response are governed by two distinct diverging length scales.

The sinusoidal forcing technique used here is not restricted to soft spheres—it can be used to test for nonlocal effects in a wide range of materials. It is straightforward to implement numerically and can also be implemented in experimental systems that allow for forcing in the bulk, such as thermoresponsive microgels

and granular monolayers. In the jamming context, obvious extensions include acoustic dispersion relations [44], nonlinear forcing [42], and steady flow [53,54].

We thank Wouter Ellenbroek and Edan Lerner for helpful discussions. We acknowledge financial support from the Netherlands Organization for Scientific Research (NWO) and the use of supercomputer facilities sponsored by NWO Physical Sciences.

*k.baumgarten@tudelft.nl

[1] L. D. Landau and E. M. Lifshitz, *Theory of Elasticity* (Butterworth-Heineman, Oxford, 1997).
[2] A. Tanguy, J. P. Wittmer, F. Leonforte, and J.-L. Barrat, Phys. Rev. B **66**, 174205 (2002).
[3] R. Maranganti and P. Sharma, Phys. Rev. Lett. **98**, 195504 (2007).
[4] W. G. Ellenbroek, E. Somfai, M. van Hecke, and W. van Saarloos, Phys. Rev. Lett. **97**, 258001 (2006).
[5] E. Lerner, E. DeGiuli, G. Düring, and M. Wyart, Soft Matter **10**, 5085 (2014).
[6] K. Karimi and C. E. Maloney, Phys. Rev. E **92**, 022208 (2015).
[7] C. S. O'Hern, L. E. Silbert, A. J. Liu, and S. R. Nagel, Phys. Rev. E **68**, 011306 (2003).
[8] M. van Hecke, J. Phys. Condens. Matter **22**, 033101 (2010).
[9] L. E. Silbert, A. J. Liu, and S. R. Nagel, Phys. Rev. Lett. **95**, 098301 (2005).
[10] M. Wyart, S. R. Nagel, and T. A. Witten, Europhys. Lett. **72**, 486 (2005).
[11] R. D. Mindlin, Arch. Ration. Mech. Anal. **16**, 51 (1964).
[12] A. C. Eringen, J. Appl. Phys. **54**, 4703 (1983).
[13] Z. P. Bazant and M. Jirásek, J. Eng. Mech. **128**, 1119 (2002).
[14] H. Askes and E. C. Aifantis, Int. J. Solids Struct. **48**, 1962 (2011).
[15] O. Pouliquen and N. Renaut, J. Phys. II (France) **6**, 923 (1996).
[16] O. Pouliquen, Y. Forterre, and S. Le Dizes, Adv. Complex Syst. **04**, 441 (2001).
[17] T. S. Komatsu, S. Inagaki, N. Nakagawa, and S. Nasuno, Phys. Rev. Lett. **86**, 1757 (2001).
[18] I. S. Aranson, L. S. Tsimring, F. Malloggi, and E. Clément, Phys. Rev. E **78**, 031303 (2008).
[19] J. Goyon, A. Colin, G. Ovarlez, A. Ajdari, and L. Bocquet, Nature (London) **454**, 84 (2008).
[20] O. Pouliquen and Y. Forterre, Phil. Trans. R. Soc. A **367**, 5091 (2009).
[21] G. Katgert, B. P. Tighe, M. E. Möbius, and M. van Hecke, Europhys. Lett. **90**, 54002 (2010).
[22] K. Nichol, A. Zanin, R. Bastien, E. Wandersman, and M. van Hecke, Phys. Rev. Lett. **104**, 078302 (2010).
[23] M. Bouzid, M. Trulsson, P. Claudin, E. Clément, and B. Andreotti, Phys. Rev. Lett. **111**, 238301 (2013).
[24] E. Wandersman and M. Van Hecke, Europhys. Lett. **105**, 24002 (2014).
[25] M. Bouzid, A. Izzet, M. Trulsson, E. Clément, P. Claudin, and B. Andreotti, Eur. Phys. J. E **38**, 125 (2015).
[26] P. Kharel and P. Rognon, arXiv:1605.00337.
[27] T. Gueudré, J. Lin, A. Rosso, and M. Wyart, arXiv: 1607.07290.
[28] L. Bocquet, A. Colin, and A. Ajdari, Phys. Rev. Lett. **103**, 036001 (2009).
[29] K. Kamrin and G. Koval, Phys. Rev. Lett. **108**, 178301 (2012).
[30] D. L. Henann and K. Kamrin, Proc. Natl. Acad. Sci. U.S.A. **110**, 6730 (2013).
[31] M. R. Kuhn, Mech. Mater. **37**, 607 (2005).
[32] B. D. Todd, J. S. Hansen, and P. J. Daivis, Phys. Rev. Lett. **100**, 195901 (2008).
[33] T. Kawasaki and L. Berthier, Phys. Rev. E **94**, 022615 (2016).
[34] D. J. Koeze, D. Vågberg, B. B. Tjoa, and B. P. Tighe, Europhys. Lett. **113**, 54001 (2016).
[35] D. Vågberg, P. Olsson, and S. Teitel, Phys. Rev. E **83**, 031307 (2011).
[36] C. E. Maloney and A. Lemaître, Phys. Rev. E **74**, 016118 (2006).
[37] B. P. Tighe, Phys. Rev. Lett. **107**, 158303 (2011).
[38] C. F. Schreck, T. Bertrand, C. S. O'Hern, and M. D. Shattuck, Phys. Rev. Lett. **107**, 078301 (2011).
[39] C. P. Goodrich, A. J. Liu, and S. R. Nagel, Phys. Rev. Lett. **109**, 095704 (2012).
[40] M. S. van Deen, J. Simon, Z. Zeravcic, S. Dagois-Bohy, B. P. Tighe, and M. van Hecke, Phys. Rev. E **90**, 020202 (2014).
[41] M. S. van Deen, B. P. Tighe, and M. van Hecke, Phys. Rev. E **94**, 062905 (2016).
[42] J. Boschan, D. Vågberg, E. Somfai, and B. P. Tighe, Soft Matter **12**, 5450 (2016).
[43] W. G. Ellenbroek, M. van Hecke, and W. van Saarloos, Phys. Rev. E **80**, 061307 (2009).
[44] S. S. Schoenholz, C. P. Goodrich, O. Kogan, A. J. Liu, and S. R. Nagel, Soft Matter **9**, 11000 (2013).
[45] E. Somfai, J.-N. Roux, J. H. Snoeijer, M. van Hecke, and W. van Saarloos, Phys. Rev. E **72**, 021301 (2005).
[46] See Supplemental Material at http://link.aps.org/supplemental/10.1103/PhysRevLett.118.098001 for the constitutive relation in tensorial form.
[47] C. P. Goodrich, S. Dagois-Bohy, B. P. Tighe, M. van Hecke, A. J. Liu, and S. R. Nagel, Phys. Rev. E **90**, 022138 (2014).
[48] E. DeGiuli, A. Laversanne-Finot, G. Düring, E. Lerner, and M. Wyart, Soft Matter **10**, 5628 (2014).
[49] W. G. Ellenbroek, Z. Zeravcic, W. van Saarloos, and M. van Hecke, Europhys. Lett. **87**, 34004 (2009).
[50] K. Karimi and C. E. Maloney, Phys. Rev. Lett. **107**, 268001 (2011).
[51] H. Mizuno, L. E. Silbert, and M. Sperl, Phys. Rev. Lett. **116**, 068302 (2016).
[52] W. Schirmacher, Europhys. Lett. **73**, 892 (2006).
[53] P. Olsson and S. Teitel, Phys. Rev. Lett. **99**, 178001 (2007).
[54] B. P. Tighe, E. Woldhuis, J. J. C. Remmers, W. van Saarloos, and M. van Hecke, Phys. Rev. Lett. **105**, 088303 (2010).